EPM/RT-85-3

THE VORTICITY-POTENTIAL METHOD FOR NUMERICAL SOLUTION OF VISCOUS DUCT FLOW IN THREE-DIMENSIONS

Herong Yang
Ricardo Camarero

Ecole Polytechnique of Montréal
February 1985

This work was carried out as part of the PRAI project no. P-8122, in collaboration with Dominion Engineering Works.

Don

Dépôt légal, 2e trimestre 1985
Bibliothèque nationale du Québec
Bibliothèque nationale du Canada

Pour se procurer une copie de ce document, s'adresser au:

Service de l'édition
Ecole Polytechnique de Montréal
Case Postale 6079, Succ. "A"
Montréal, Québec H3C 3A7

(514) 340-4903

Compter 0,05$ par page (arrondir au dollar le plus près), plus 1,50$ (Canada) ou 2,50$ (étranger) pour la couverture, les frais de poste et la manutention. Régler en dollars canadiens par chèque ou mandat-poste au nom de l'Ecole Polytechnique de Montréal. Nous n'honorerons que les commandes accompagnées d'un paiement, sauf s'il y a eu entente préalable, dans le cas d'établissements d'enseignement ou d'organismes canadiens.

ABSTRACT

A method is presented for the numerical solution of three-dimensional, viscous incompressible steady-state duct flow. The governing equations are solved in non-primitive variables: vector potential, scalar potential and vorticity, using a finite difference technique. The solution procedure involves a combination of a potential solution and an iterative cycling between the vorticity transport equation and the vector potential equation. The numerical solution is obtained on a body-fitted coordinate grid by the line successive overrelaxation scheme. The method is applied to the calculation of flow in a square elbow and in a twisted square elbow. The results are compared with other numerical solutions, and experiments. It is concluded that the proposed method could have useful applications in the simulation of duct flows with Reynolds number of about 100.

NOMENCLATURE

A	Vector Potential Function
Cp	Pressure Coefficient
n	Unit Vector Normal to Boundaries
p	Static Pressure
Re	Reynolds Number

V	Velocity Vector Variable
V_*	Mean Velocity at the Inlet of Duct
W	Vorticity Vector Variable
x, y, z	Cartesian Coordinates in Physical Domain
ξ, η, ζ	Body-Fitted Coordinates in Numerical Domain
ϕ	Scalar Potential Function
τ_1, τ_2	Unit Vectors Tangential to Boundaries
ω	LSOR Parameter

Subscripts

i, j, k	Value of a Variable at a Grid Point
n	Normal Component
x, y, z	Components of a Vector in Cartesian System
τ	Tangential Component

1. INTRODUCTION

In recent years, a number of numerical methods have been developped for three-dimensional flow simulation. The accuracy and efficiency of a method with which various flow phenomena can be simulated depend directly on the choice of a mathematical model and the design of a numerical solution procedure. Three-dimensional methods can be classified into two main categories according to the choice of the calculation variables.

1. Methods using primitive variables. In these methods, the governing equations are solved in terms of the velocity and the pressure. Two of the main difficuties inherent in determining the velocity and the pressure are, first, that the momentum equation has to be solved subject to the continuity equation, and second, that there is no evolution equation for the pressure. The first attempts at resolving these difficuties lead to instabilities in the numerical calculations of the complete Navier-Stokes equations.

Recently, a so-called "parabolic method" has been studied by a number of investigators, such as Moore and Moore (1), Pratap and Spalding (2) and Briley (3). In this method, the Navier-Stokes equations are simplified by neglecting the diffusion term in the main flow direction and hence become elliptic in the transverse plane and parabolic in the main flow direction. A forward space marching technique can then be used, since it is supposed that the downstream effects are transmitted only via the cross-section pressure variation. This method requires significantly less computer expences, but it is limited by the assuming of a predominant flow direction. Consequently it is restricted to the situations in which there is negligible reverse flow.

2. Methods using nonprimitive variables. A remarkable method in this class is known as the vorticity-potential method, which can be regarded as the three-dimensional generalization of the

two-dimensional vorticity-stream method. The approach is based on the work of such authors as Hirasaki and Hellums (4) and (5), Aziz and Hellums (6). The velocity is decomposed into two parts: a potential part which is expressed as the gradient of the scalar potential, and a rotational part which is expressed as the curl of the vector potential. The basic equations are then transformed to decouple the pressure from the velocity field. This yields the vorticity as the main variable instead of velocity. In the past, a number of developments on the numerical solutions of three-dimensional flow problems using the vorticity-potential method have been proposed. Most of these however concern rather simple flow geometries. For example, Aziz and Hellums (6) have tested a natural convection in a box, flow in a square duct has been studied by Areqbesola and Burley (7) and flow in the straight duct with an obstruction has been simulated by Lacroix, Camarero and Tapucu (8). Furthermore, most of them encounted a common difficulty in setting the boundary conditions on the vector potential in the most natural form.

The objective of the present study is to pursue this approach with particular attention on two basic issues: 1) correct implementaion of the boundary conditions on the scalar and vector potentials, 2) the possibility of application of this method for complicated flow geometries.

2. GOVERNING SYSTEM OF DUCT FLOW

The system of dimensionless equations describing a viscous incompressible steady-state flow in vector form is

$$\nabla \cdot V = 0 \tag{1}$$

$$(V\nabla)V = -\nabla p + \frac{1}{Re}\nabla^2 V \tag{2}$$

where V is the velocity, p is the static pressure and Re is the Reynolds number.

The present method is based on the decomposition of the overall velocity V into an irrotational flow part and a rotational flow part:

$$V = -\nabla\phi + \nabla \times A \tag{3}$$

where ϕ is the scalar potential, A is the vector potential. Using this potential-decomposition and the vorticity W, defined by:

$$W = \nabla \times V \tag{4}$$

the governing system (1-2) can be replaced by the following system.

$$(V\nabla)W - (W\nabla)V = \frac{1}{Re}\nabla^2 W \tag{5}$$

$$\nabla^2\phi = 0 \tag{6}$$

$$\nabla \cdot A = 0 \tag{7}$$

$$\nabla^2 A = -W \tag{8}$$

Hirasaky and Hellums (4) have given a boundary condition set for system (5-8):

$$\frac{\partial \phi}{\partial n} = -n \cdot V$$

$$\frac{\partial A_n}{\partial n} = 0 \qquad (9)$$

$$A_{\tau_1} = 0, \quad A_{\tau_2} = 0$$

$$W = \nabla \times V$$

where n is the unit vector normal to the boundaries, τ_1 and τ_2 are the unit vectors tangent to the boundaries. It should be pointed out that with this set of boundary conditions the solenoidal condition Eq.(7) on the vector potential can be removed from the system (5-8) (see Ref.(4)).

In this set of boundary conditions, the normal velocities on the boundaries are satisfied by the potential velocity $-\nabla\phi$ from

$$\frac{\partial \phi}{\partial n} = -n \cdot V$$

and are not altered by the vector potential as can be seen from

$$(\nabla \times A)_n = c\left(\frac{\partial A_{\tau_2}}{\partial \tau_1} - \frac{\partial A_{\tau_1}}{\partial \tau_2}\right) = 0$$

where c is a geometry coefficient. This seems not natural, if the normal velocity distribution on a boundary is not irrotational. Typically, in a duct flow problem, the inlet section is flat, and the inlet velocity has a parabolic profile. In this case, the po-

tential solution process is difficult, because of the rotational inlet condition.

A new set of boundary conditions is proposed for the duct flow simulation, in the present method.

On the solid walls and the inlet:

$$\frac{\partial \phi}{\partial n} = 0 \qquad \text{(on the walls)}$$

$$\frac{\partial \phi}{\partial n} = -V_* \qquad \text{(on the inlet)}$$

$$\nabla \cdot A = 0 \qquad (10)$$

$$A_\tau = \tau \, (\nabla \times B)$$

$$W = \nabla \times V$$

at the outlet:

$$\frac{\partial \phi}{\partial n} = -V_*$$

$$\frac{\partial^2 A}{\partial \zeta^2} = 0 \qquad (11)$$

$$\frac{\partial^2 W}{\partial \zeta^2} = 0$$

where V_* is the mean velocity at the inlet of duct.

The vector B is introduced only for the boundary conditions,

and it satisfies the following equations:

$$\begin{aligned} \nabla_s^2 B_n &= -n\,V + V_* && \text{(on the inlet)} \\ B_c &= 0 && \\ B &= 0 && \text{(on the walls)} \end{aligned} \qquad (12)$$

where ∇_s^2 is the Laplace operator on a surface. A detailled discussion of vector B can be found in Ref.(5). For a flat inlet section, the surface operator ∇_s^2 becomes the usual two-dimensional Laplace operator. For instance, if the inlet is a rectangular section in the x-y plane, the vector B can be solved from:

$$\nabla^2 B_z = -V_z +$$

$$B_x = 0, \quad B_y = 0$$

$$\frac{\partial B_z}{\partial x} = 0 \qquad x = x_{min},\ x_{max}$$

$$\frac{\partial B_z}{\partial y} = 0 \qquad y = y_{min},\ y_{max}$$

In order to remove the specification of the velocities on the oulet section, an extrapolation technique is applied on the boundary conditions (11), which requires that the flow must keep going steadily along the flow direction in the outlet region.

3. CURVILINEAR COORDINATE SYSTEM

In order to facililate the treatment of the boundary conditions for a general curved duct, the Cartesian coordinate system (x,y,z) is transformed to a body-fitted curvilinear coordinate

system (ξ, η, ζ). The coordinate ζ is set along the primary flow direction, ξ and η are the cross stream directions. The body-fitted grids are generated by the solution of a non-linear system of elliptic equations, Ref.(9)

In the curvilinear coordinate system, the transformed equations of (5), (6) and (8) can be written in a common form:

$$C_{11}\frac{\partial^2 f}{\partial \xi^2} + C_{12}\frac{\partial^2 f}{\partial \eta^2} + C_{13}\frac{\partial^2 f}{\partial \zeta^2} + 4C_{21}\frac{\partial^2 f}{\partial \eta \partial \zeta} + 4C_{22}\frac{\partial^2 f}{\partial \xi \partial \zeta} +$$

$$4C_{23}\frac{\partial^2 f}{\partial \xi \partial \eta} + 2C_{31}\frac{\partial f}{\partial \xi} + 2C_{32}\frac{\partial f}{\partial \eta} + 2C_{33}\frac{\partial f}{\partial \zeta} + \qquad (13)$$

$$2C_1'\frac{\partial f}{\partial \xi} + 2C_2'\frac{\partial f}{\partial \eta} + 2C_3'\frac{\partial f}{\partial \zeta} = S$$

where f may represent any one of ϕ, A_x, A_y, A_z, W_x, W_y and W_z.

The coefficients C_{ij}, i=1, 2, 3; j=1, 2, 3 are obtained from the Laplace operator:

$$C_{1j} = \left(\frac{\partial \xi_i}{\partial x}\right)^2 + \left(\frac{\partial \xi_i}{\partial y}\right)^2 + \left(\frac{\partial \xi_i}{\partial z}\right)^2$$

$$C_{2j} = 0.25\left(\frac{\partial \xi_i}{\partial x}\frac{\partial \xi_k}{\partial x} + \frac{\partial \xi_i}{\partial y}\frac{\partial \xi_k}{\partial y} + \frac{\partial \xi_i}{\partial z}\frac{\partial \xi_k}{\partial z}\right) \qquad (14)$$

i,j,k is a permutation

$$C_{3j} = 0.5\left(\frac{\partial^2 \xi_i}{\partial x^2} + \frac{\partial^2 \xi_i}{\partial y^2} + \frac{\partial^2 \xi_i}{\partial z^2}\right)$$

where ξ_1, ξ_2 and ξ_3 are present ξ, η and ζ respectively.

While the formulas of C_1', C_2', C_3' and S are listed in the following table:

f	C_j	S
ϕ	0	0
A_i	0	$-W_i$
W_i	$-0.5\,Re(V_x\frac{\partial \xi_j}{\partial x} + V_y\frac{\partial \xi_j}{\partial y} + V_z\frac{\partial \xi_j}{\partial z})$	$Re(-W_x\frac{\partial V_i}{\partial x} - W_y\frac{\partial V_i}{\partial y} - W_z\frac{\partial V_i}{\partial z})$

where i represents one of the subscripts x, y and z.

4. FINITE DIFFERENCE APPROXIMATION

With the body-fitted coordinate system, the calculation domain can be discretized uniformly, $d\xi=1$, $d\eta=1$, $d\zeta=1$, $\xi\,min=1$, $\eta\,min=1$ and $\zeta\,min=1$. In such a uniform mesh, the finite difference approximation of Eq.(16) is

$$(C_{11} + C_{31} + C_1')f_{i+1jk} + (C_{11} - C_{31} - C_1')f_{i-1jk} +$$

$$
\begin{aligned}
&(C_{12} + C_{32} + C_2) f_{ij+1k} + (C_{12} - C_{32} - C_2) f_{ij-1k} + \\
&(C_{13} + C_{33} + C_3) f_{ij k+1} + (C_{13} - C_{33} - C_3) f_{ij k-1} + \\
&2(C_{11} + C_{12} + C_{13}) f_{ijk} + \\
&(f_{ij+1k+1} - f_{ij-1k+1} - f_{ij+1k-1} + f_{ij-1k-1}) C_{21} + \\
&(f_{i+1jk+1} - f_{i+1jk-1} - f_{i-1jk+1} + f_{i-1jk-1}) C_{22} + \\
&(f_{i+1j+1k} - f_{i-1j+1k} - f_{i+1j-1k} + f_{i+1j+1k}) C_{23} = S
\end{aligned}
\tag{15}
$$

where the subscripts i, j and k refer to the coordinates ξ, η and ζ respectively.

In the present study, the boundary condition for scalar potential is treated implicitly. For $f = \phi$, the discretizing points (i,j,k) of Eq.(16) include all boundary points. The fictitious points, points outside the domain, involved in Eq.(16) can be eliminated by the boundary equation, which has the following approximation form:

$$
2Cs_1 \frac{\partial \phi}{\partial \xi} + 2Cs_2 \frac{\partial \phi}{\partial \eta} + 2Cs_3 \frac{\partial \phi}{\partial \zeta} = Cs_4 \tag{16}
$$

$$
\begin{aligned}
Cs_1 &= 0.5\left(n_x \frac{\partial \xi}{\partial x} + n_y \frac{\partial \xi}{\partial y} + n_z \frac{\partial \xi}{\partial z}\right) \\
Cs_2 &= 0.5\left(n_x \frac{\partial \eta}{\partial x} + n_y \frac{\partial \eta}{\partial y} + n_z \frac{\partial \eta}{\partial z}\right) \\
Cs_3 &= 0.5\left(n_x \frac{\partial \zeta}{\partial x} + n_y \frac{\partial \zeta}{\partial y} + n_z \frac{\partial \zeta}{\partial z}\right)
\end{aligned}
\tag{17}
$$

where $(n_x, n_y, n_z) = n$ is the unit vector normal to the boundaries.

The values of the vector potential A on the walls and the inlet section are calculated explicitly, from an algebraic system at each boundary point for the three components of A. This system can be expressed as

$$\begin{aligned} \tau_{1x} A_x + \tau_{1y} A_y + \tau_{1z} A_z &= q_1 \\ \tau_{2x} A_x + \tau_{2y} A_y + \tau_{2z} A_z &= q_2 \\ Ca_1 A_x + Ca_2 A_y + Ca_3 A_z &= Ca_4 \end{aligned} \qquad (18)$$

where q_1 and q_2 are defined by the boundary equations (10)

$$q_1 = \tau_1 (\nabla \times B)$$

$$q_2 = \tau_2 (\nabla \times B)$$

τ_1 and τ_2 are the unit tangential vectors. The coefficients Ca_1, Ca_2, Ca_3 and Ca_4 are determined by the finite difference approximation of the solenoidal condition on the boundaries.

The approximation of the extrapolation condition on the section next to the outlet gives:

$$A_{o\,kmax} = 2A_{o\,kmax-1} - A_{o\,kmax-2} \qquad (19)$$

The boundary values of the vorticity W is simply calculated from Eq.(4) on the walls and on the inlet. The outlet boundary condition is analogous to that of the vector potential.

5. SOLUTION PROCEDURE

The overall solution procedure consists of the following steps:

(1). Generation of the body-fitted grid, the coordinate transformation data, such as the Jacobian matrix, and the coefficients of the Laplace operator.

(2). Specification of the inlet velocity profile, calculation of the boundary equation coefficients for the scalar potential, and and calculation of the values of vector potential on the inlet.

(3). Computation of the scalar potential from Eq.(6) to the desired accuracy.

(4). Cycling the iterative computations between the vorticity transport equation (5) and the vector potential equation (8) until a stable velocity field is reached.

(5). Visualization of the flow pattern by the vector fields of the velocity and the vorticity, streamlines and contours of velocity components.

Step (1) requires a body-fitted grid generation program, which creates the grid data from the boudary geometry, and the transformation coefficients. In order to maintain a second order accuracy in the entire procedure, all the derivatives involved

are approximated by the central or one-side difference formulas.

In step (3), a linear initialization technique is applied in the scalar potential solution. Using the mass conservation, an initial velocity field can be proposed such that, its direction is perpendicular to the section surface and its magnitude is constant in one section to satisfy the continuity, i.e.

$$V^{in} = n\ (V_*(\text{area of inlet}) / (\text{area of section})) \qquad (20)$$

where n is the unit vector normal to the section. Therefore, the scalar potential is initialized through the following equations:

$$\nabla\phi = -V^{in}$$

$$\frac{\partial\phi}{\partial\xi} = \frac{\partial x}{\partial\xi}\frac{\partial\phi}{\partial x} + \frac{\partial y}{\partial\xi}\frac{\partial\phi}{\partial y} + \frac{\partial z}{\partial\xi}\frac{\partial\phi}{\partial z} \qquad (21)$$

$$= -\frac{\partial x}{\partial\xi}V_x^{in} - \frac{\partial y}{\partial\xi}V_y^{in} - \frac{\partial z}{\partial\xi}V_z^{in}$$

In step (3) and (4), a line relaxation scheme is used to obtain solutions of the scalar potential, the vector potential and the vorticity field. The direction of relaxation sweep is along the primary flow direction, the ξ direction, section by section. Within each section, the relaxation is performed in the η direction line by line, each line in ξ direction is treated implicitly as a block.

There are five sub-steps in step (4), the cycling step:

(a). Calculation of new boundary values of vorticity from the current velocity values.

(b). Computation of the new values of the vorticity at interior points from the vorticity transport equation for a few iterations.

(c). Computation of new values of the vector potential at interior points with the current values of the vorticity by a few iterations.

(d). Calculation of new boundary values of the vector potential from the boundary equations.

(e). Modification of the velocity from the current values of the vector potential, and beginning a new cycle.

6. SIMULATION OF FLOW IN A SQUARE ELBOW

To test the general capabilities of the proposed method, the first numerical experiment is designed to simulate the viscous flow in an elbow with square cross section. All the calculations were performed on the IBM-4341-II computer. To investigate the effects of Reynolds number, two cases of $Re = 10$ and $Re = 80$

are compared, in each case the corresponding Dean numbers, defined as

$$De = Re \sqrt{H/R_m}$$

are 6.32456 and 50.5964, where H = 1 is the radial distance of the elbow, and R_m = 2.5 is the channel mean radius of curvature. The upstream and downstream tangents (the lengths of straight ducts attached to the curved duct) are 0.349H and 0.524H respectively. The elbow is turned by 60 degrees, as shown in Fig.1. Uniform 11x11 grids are used at each cross section, and 21 streamwise sections are required along the channel.

For computational economy, the velocity profile at the inlet is assumed to be parabolic with null transverse components, i.e.

$$\begin{aligned} V_x &= 36.0\ y\ z\ (1-y)\ (1-z) \\ V_y &= 0 \\ V_z &= 0 \end{aligned} \qquad (26)$$

which is similar to the fully developed velocity profile, given by Han (10) in a square duct.

A satisfactory potential solution requires 300 iterations and 10 minutes of CPU. This is identical to 7.87×10^{-4} seconds per iteration per point. The residual history is shown in Fig.2. The first 20 iterations form a steep decreasing part with a mean reduction factor f_r, defined as

$$Res^{(n+m)} = f_r^m\ Res^{(n)} \qquad (27)$$

of 0.666. Then it decreases with f_r = 0.965 until the 250-th

iteration. The streamwise profile of the potential velocity at the location of θ =32 (θ is the angle of turning) is compared with the analytical solution of free vortex motion in Fig.3, which illustrates the accuracy of the potential solution. The distribution of pressure coefficient Cp calculated from:

$$Cp = 1.0 - |V|^2 / V_*^2 \qquad (28)$$

is shown in Fig.4 by the contours of constant values.

To add the viscous influence with Re = 80, 60 cycles of computations between the vorticity transport equation and the vector potential equation were performed. The run time is about 8.66x10 seconds per cycle per point.

The results are presented in Figs.5 to 8. The three-dimensional nature of the flow is presented by means of persperctive of the velocity field on two η = constant surfaces in Fig.5. The development of streamwise velocity profiles are presented in Fig.6. The curvature has little effect on the streamwise velocities near the section of θ =0. However the thick boundary layer in this region generates a rapid and strong secondary flow as shown in Fig.8. As the flow progresses downstream, the radial profiles become more asymmetric, which can be directly related to the helical motion formed by the secondary flow as it moves downstream. The helical motion draws low momentum fluid from the side walls and convects it toward regions adjacent to the suction surface. High streamwise velocities existing near the channel

center are moved accordingly toward the pressure surface as indicated in Fig.6. The presence of a flat region in the center of the vertical profiles near the exit is also a manifestation of the helical motion.

To assess the accuracy of the present solution, the computed fully developed streamwise velocity profile is compared in Fig. 7 with other prediction of viscous flow with Re = 205 computed by Khalil and Weber (11) from parabolized Navier-Stokes equation, and with experimental measurements obtained by Mori et al (12). Examination of this figure shows qualitative agreement. The differences observed betweem the two computed solutions reflect the difference in Reynolds number and as well as the difference in these methods.

The development of secondary flow is clearly illustrated in Fig.8. The helical motion originates at location $\theta = 8$ from the beginning of channel turning. At the exit, the secondary flow does not disappear entirely, because the downstream tangent is relatively short, and it would require a length of $0.07Re = 5.6$ for the re-development of the flow. The centers of the streamwise vortices are symetrically located about the central plane in the upstream part. As the flow progresses, these centers move symetrically towards the pressure surface drawn by the strong radial flow in the central plane.

With the same flow parameters as above, and a fine mesh of 11x11x41, the flow is recomputed to test the response of the present model to the grid size. A fine grid requires more relaxation sweeps for the boundary condition to penetrate to the interior of the domain, and hence the overall convergence speed is lower. Furthermore, the computer time spend on each sweep for the fine mesh is also more than that for the coarse mesh. On the other hand, the fine mesh should give a more accuarate solution since the numerical error is mainly depend on the length of the segment in the mesh. However, in the present case, the fine mesh does not significiently improve the solution, because the solution on the coarse mesh is sufficiently accurate.

For the purpose of checking the response of the present model to differences in Reynolds number, a solution at Re = 10 was computed. With this low Reynolds number, the parabolic velocity profile at the inlet maintains the same shape as the flow turning along the circular arc due to the strong effects of the viscosity. This is shown in Fig. 10. Radial motion nearly disppeares. Actually, the transverse component of the velocity is less than 5 percent of the streamwise component.

8. SIMULATION OF FLOW IN A TWISTED ELBOW

The aim of this method is the simulation of three-dimensional

viscous flow in an arbitrary channel, so the second numerical application is devoted to show the fully three-dimesional characteristics of present method.

The channel, shown in Fig.11, is a 60 degree turning elbow with 60 degree twist around its central line. The cross section is a square. The body-fitted mesh points in the turning part are obtained analytically by the following formulas:

$$x = r'\sin\theta$$

$$y = r'\cos\theta$$

$$z = z' \qquad (29)$$

and

$$r' = (r - R_m)\cos\theta - (z - z_m)\sin\theta + R_m$$

$$z' = (r - R_m)\sin\theta - (z - z_m)\cos\theta + z_m$$

where R is the radius of curvature of the central line in the channel, z_m is the location of surface $\xi = 0.5(\xi_{min} + \xi_{max})$ in the z direction at the beginning of the turning part. In order to observe the recovery of the streamwise velocity profile downstream of the turning, a longer downstream tangent of length 2.1H is used in this test. The upstream tangent is 0.524H long. Here H=1 is the side of the cross section.

The 11x11 mesh is used again for each cross section, and the total number of sections is 31, including 16 sections in the turning part. The increments of both turning and twisting angles between two sections are 4 degrees.

A parabolic velocity profile is applied at the inlet as for the previous test. The potential solution, obtained after 300 iterations with an overrelaxation parameter 1.6, costs about 20 minutes of computer time. The residual is less than 10^{-2}. The potential velocity on the boundary surfaces of the channel is shown in Fig.12. One can observe that the condition of tangency is well applied. As in the previous test, the potential pressure coefficient Cp is plotted in Fig.13 in contours of constant values.

A viscous solution was obtained for Re=80 after 200 iteration cycles, which cost about 109 minutes, or 8.72×10^{-3} seconds per cycle per point. The convergence behaviour is shown in Fig.14. It should be noted that such long CPU time will not required in general. In the present case this was done to show that the solution process is convergent. Usually 60 cycles will yield sufficiently accurate solutions for numerical prediction, and this costs about 37 minutes. The following results were all obtained after 60 cycles.

The velocity distribution is shown in Fig.15, which presents the velocity field in ξ =constant surface with the channel configuration.

The most interesting physical phenomena in such a complex

geometry is the development of secondary flow, which is presented in Fig.16. It consists of a vortex pair formed at location around $\theta = 15°$. The vortex pair remains perpendicular to the plane of channel turning as it moves downstream. The twisting of the cross section seems to have no effect on the location of the vortices, because it is generated by the turning of primary flow only. However twisting does increase the strength of one side of the vortex pair, and decrease that of other side. This influence is more evident after $\theta = 40°$. After the channel stops turning and twisting at $\theta = 60°$, the flow begins to recover to the straight channel flow type. The vortex pair is felt up to 1.7H downstream of the end of turning part.

ACKNOWLEDGMENTS

This research was carried out under the grants P-8122 from NSEC of Canada and the scholarship from the goverment of China.

REFERENCES

1. J. Moore and J.G. Moore
A Calculation Procedure for Three-dimensional, Viscous, Compressible Duct Flow
Journal of Fluids Engineering, Vol.101, pp.415-428, 1979

2. V.S. Pratap and D.B. Spalding

Fluid Flow and Heat Transfer in Three-Dimensional Duct Flows

Int. J. Heat Mass Transfer, Vol.19, pp.1183-1188, 1976

3. W.R Briley

Numerical Method for Predicting 3d Steady Viscous Flow in Ducts

J. Comp. Phys., Vol.14, p.8, 1974

4. G.J. Hirasaki and J.D. Hellums

Boundary Conditions on The Vector and Scalar Potentials in viscous three-Dimensional Hydrodynamics

Quarterly of Applied Mathematics, Vol.28, pp.293-296, 1970

5. G.J. Hirasaki and J.D. Hellums

A General Formulation of The Boundary Conditions on The Vector Potential in Three-Dimensional Hydrodynamics

Quarterly of Applied Mathematics, Vol.26, pp.331-342, 1968

6. K. Aziz and J.D. Hellums

Numerical Solution of The Three-Dimensional Equations of Motion for Laminar Natural Convection

The Physics of Fluids, Vol.10, pp.314-324, 1967

7. Y.A.S. Aregbesola and D.M. Burley

The Vector and Scalar Potential Method for The Numerical Solution of Two-and Three-Dimensional Navier-Stokes Equations
Journal of Computational Physics, Vol.24, pp.398-415, 1977

8. M. Lacroix, R. Camarero and A. Tapucu
Etudie d'Ecoulements Internes Tridimensionnels
Rapport Technique of Ecole Polytechnique de Montreal,
EP84-R-9, 1984

9. R.Camarero and M. Reggio
A Multigrid Scheme for Three-Dimensional Body-Fitted Coordinates in Turbomachine Applications
J. of Fluids Engineering, ASME, Vol.105, PP.76-82, 1983

10. L.S. Han
Hydrodynamic Entrance Lengths for Incompressible Laminar Flow in Rectangular Ducts
J. Appl. Mech., Vol.27, pp.403-409, 1960

11. I.M. Khanlil and H.G. Weber
Modeling of Three-dimensional Flow in Turning Channels
ASME J. OF Eng. for Turbines and Power,
Vol.106, pp.682-691, 1984

12. Y. Mori, Y. Uchida and T. Ukon
Forced Convective Heat Transfer in a Curved Channel with a

Square Cross Section

Int. J. Heat and Mass Transfer, Vol.14, p.1787, 1971

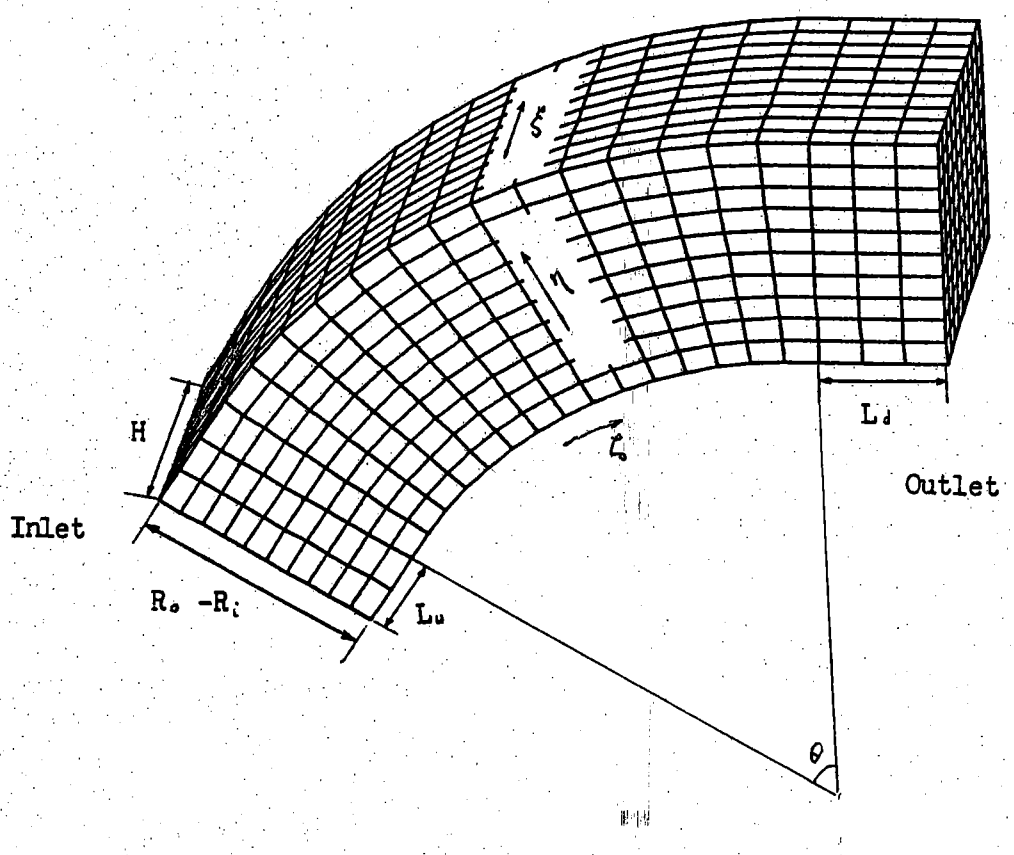

Fig.1 Description of the Square Elbow

$R_i = 2.0$, $R_o = 3.0$

$L_u = 0.349$, $L_d = 0.524$

$H = 1.0$, $\theta = 60$

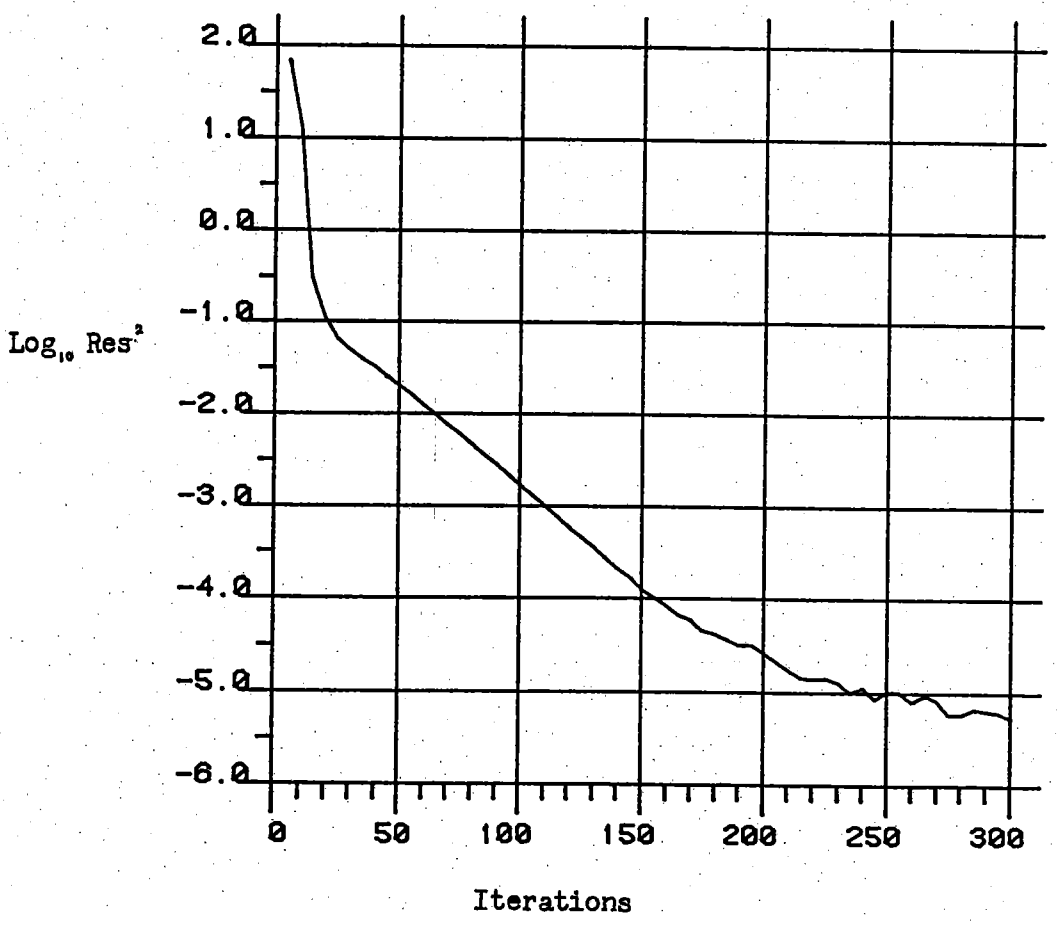

Fig.2 Residual History of ϕ's Eq.

Mesh = 11x11x21, ω = 1.6

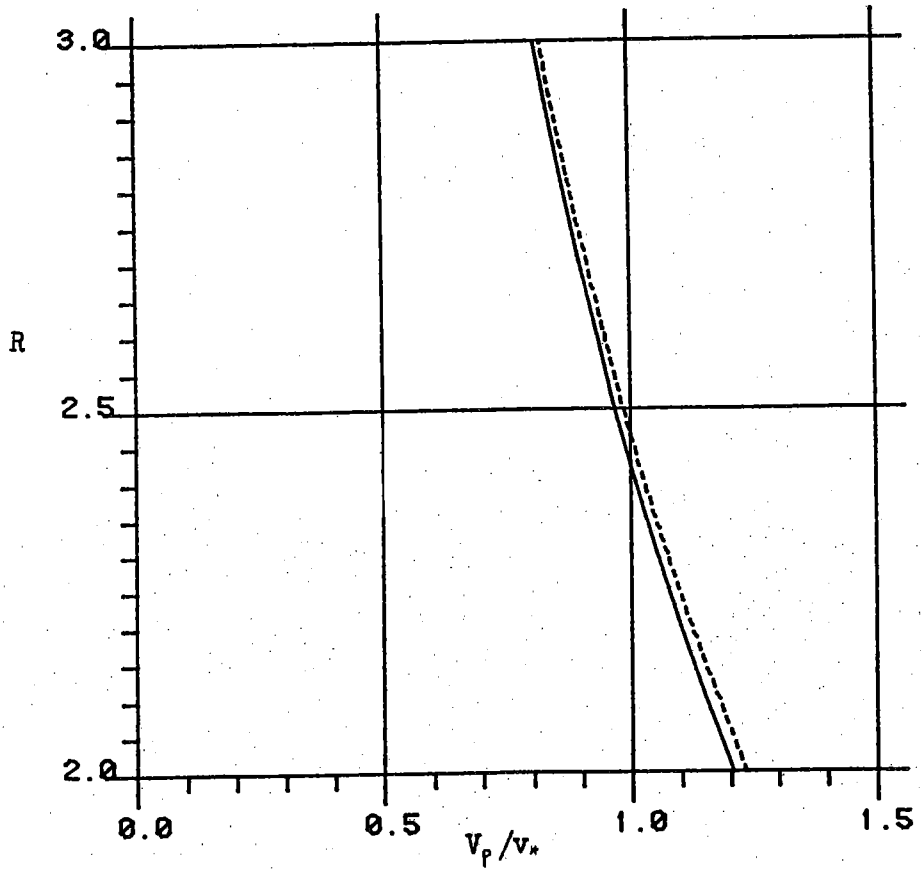

Fig.3 Streamwise Profile of Potential Velocity

Mesh = 11x11x21, Location of $\theta = 32^\circ$

——— Present Results

------ Analytical Results

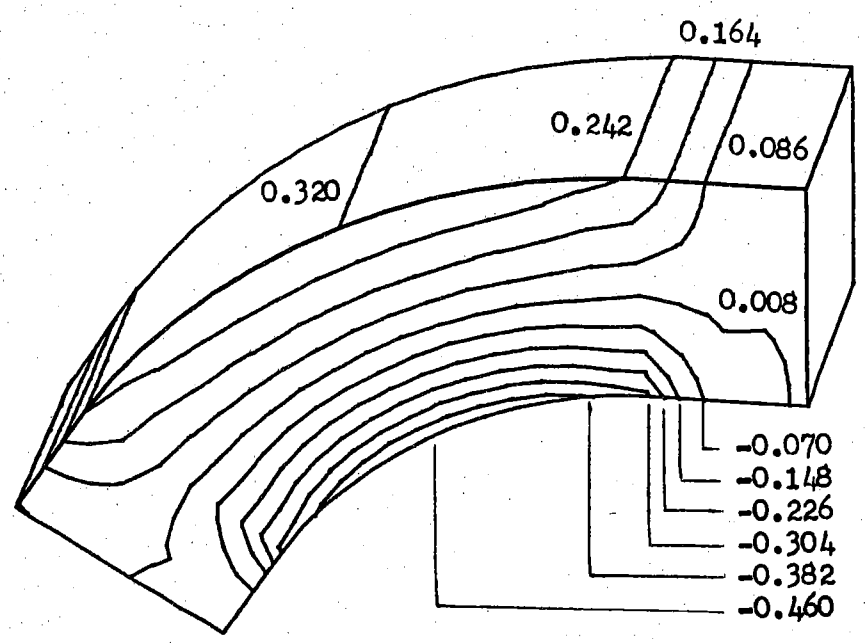

Fig.4 Distribution of Potential Pressure Coefficient Cp

Mesh = 11×11×21

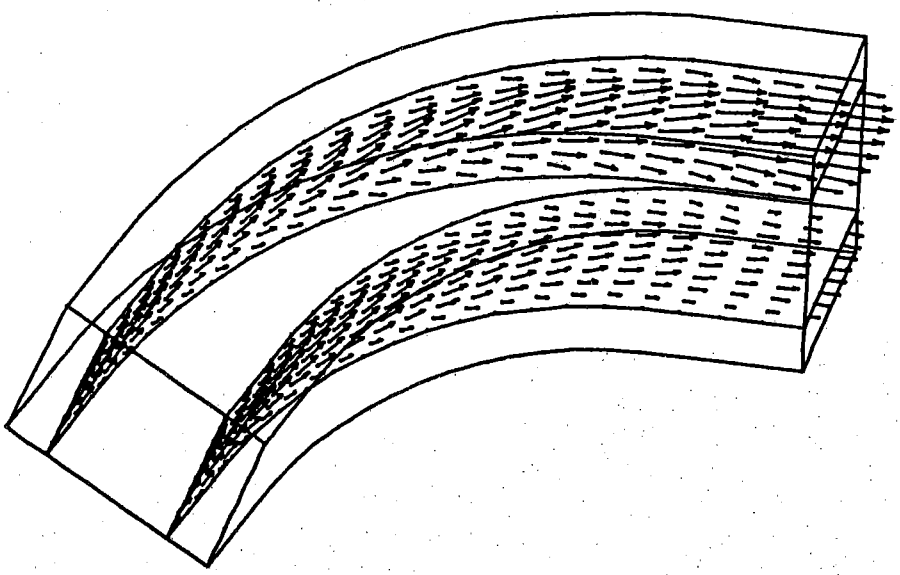

Fig.5 3-D View of Flow Pattern

Mesh = 11x11x21, Re = 80

Scale of V/V_* → = 1.0

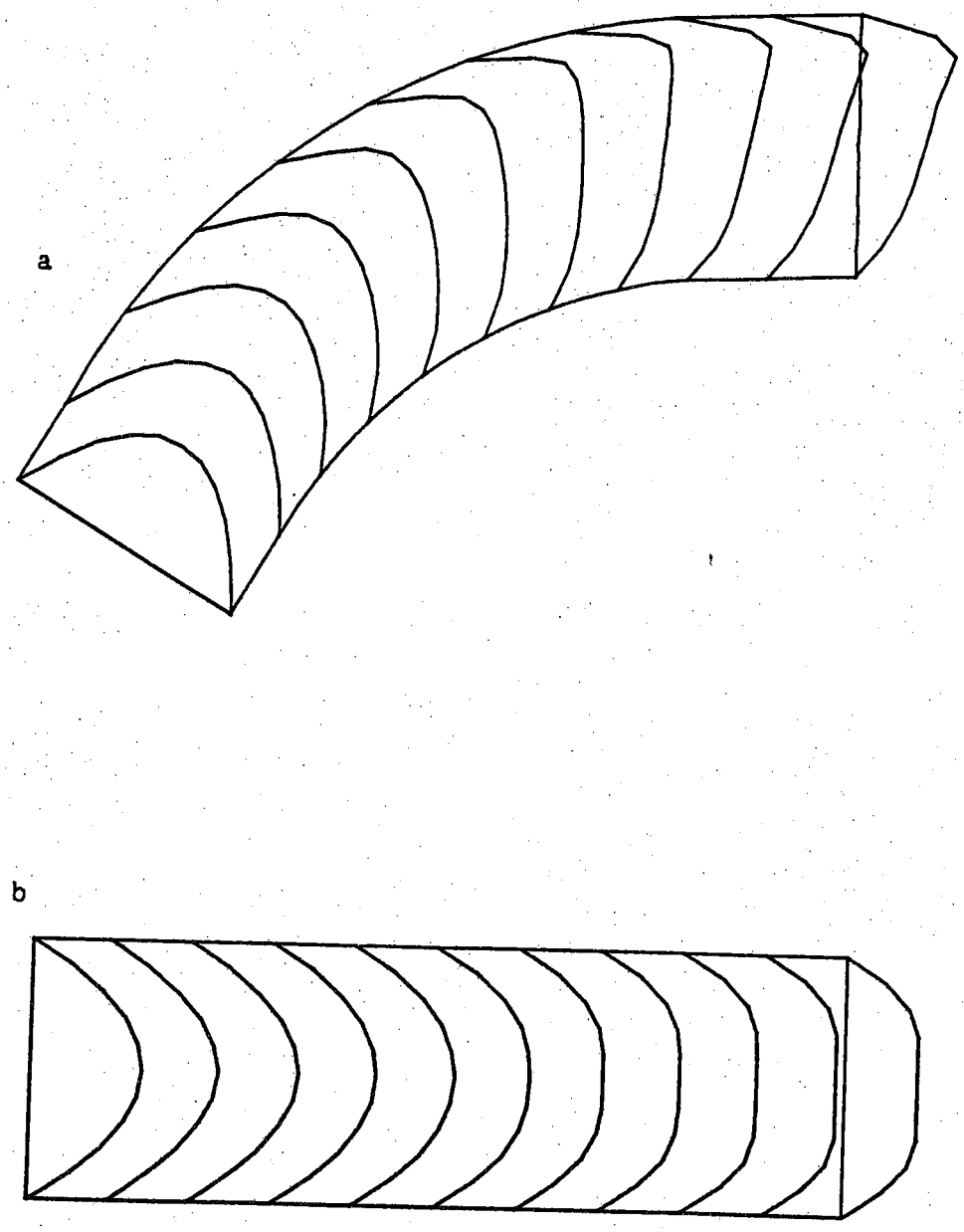

Fig.6 Development of Streamwise Velocity Profile

Mesh = 11x11x21, Re = 80

a. In the Plane of z = 0.5

b. In the Surface of r = 2.5

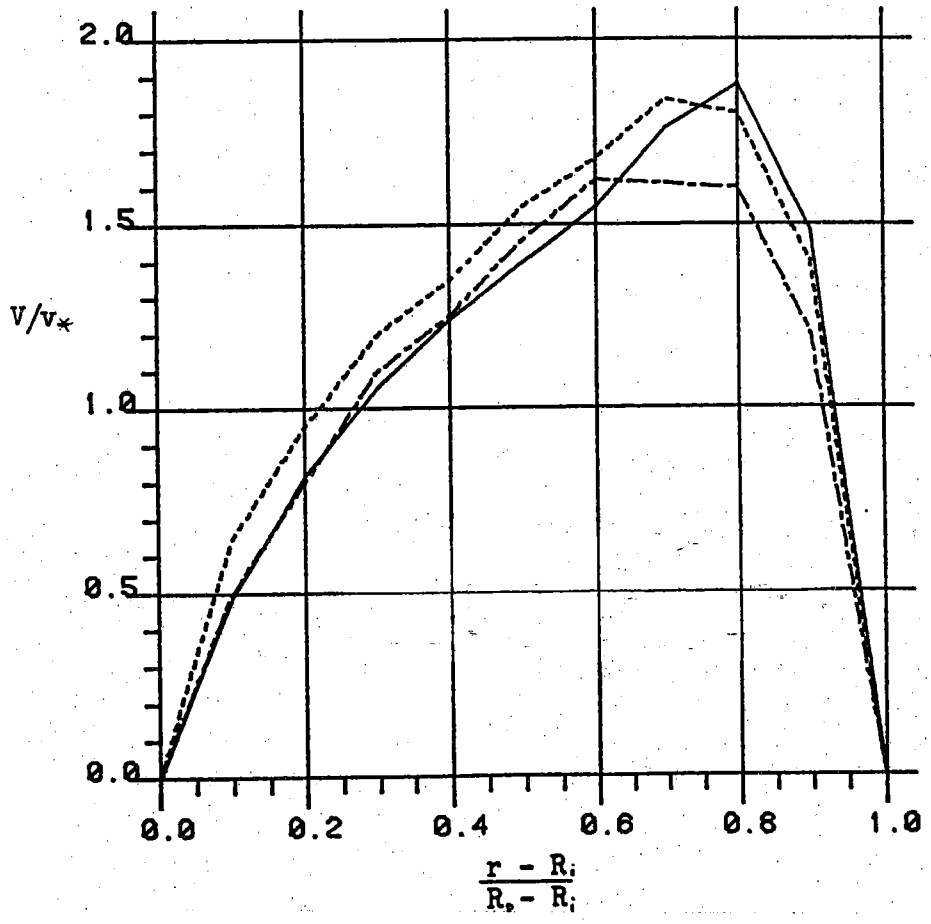

Fig.7 Fully Developed Velocity Profile

Mesh = 11x11x21

——— Present Results

----- Khalil Computed Results

—·—·— Mori Masured Results

a.

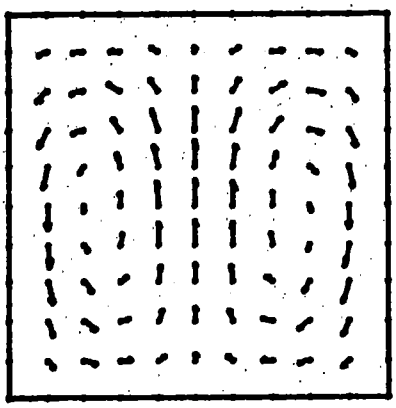

b.

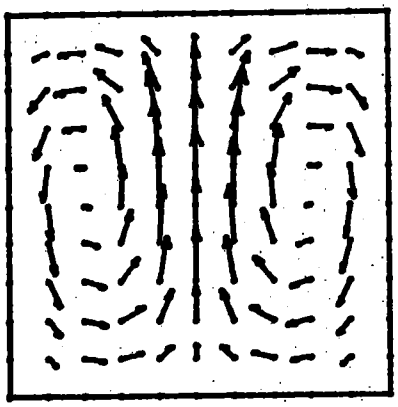

c.

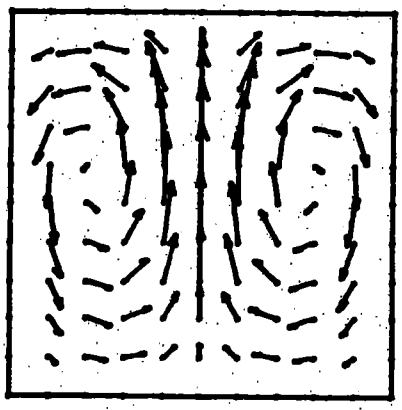

d.

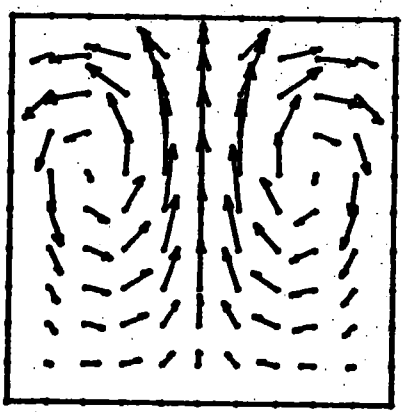

e.

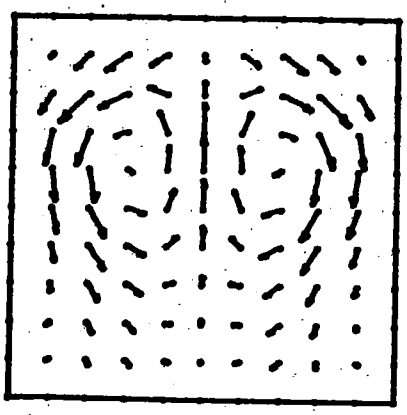

Fig.8 Development of Secondary Flow

Mesh = 11×11×21, Re = 80

Scale of V/V_* ⟶ = 0.2

a. In the Section of $\theta = 8^\circ$

b. In the Section of $\theta = 24^\circ$

c. In the Section of $\theta = 40^\circ$

d. In the Section of $\theta = 56^\circ$

e. In the Outlet

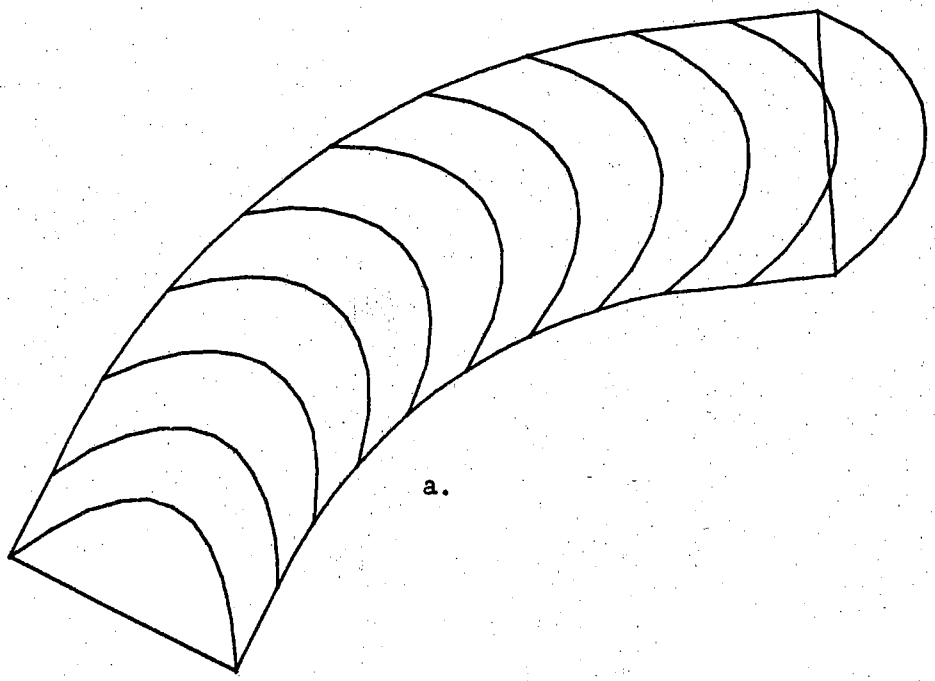

a.

b.

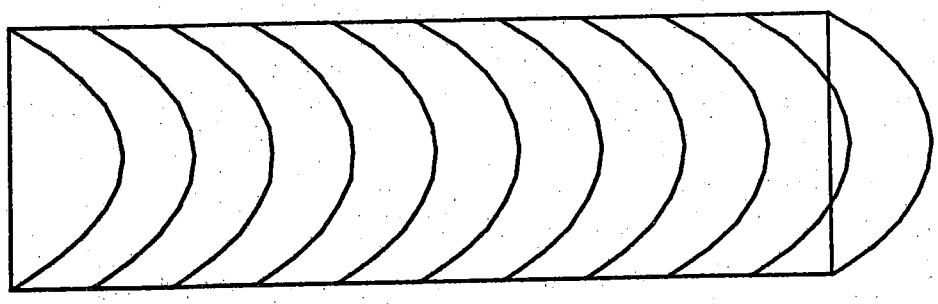

Fig.9 Streamwise Velocity Profiles with Low Re

Mesh = 11x11x21, Re = 10

a. In the Plane of z = 0.5

b. In the Surface of r = 2.5

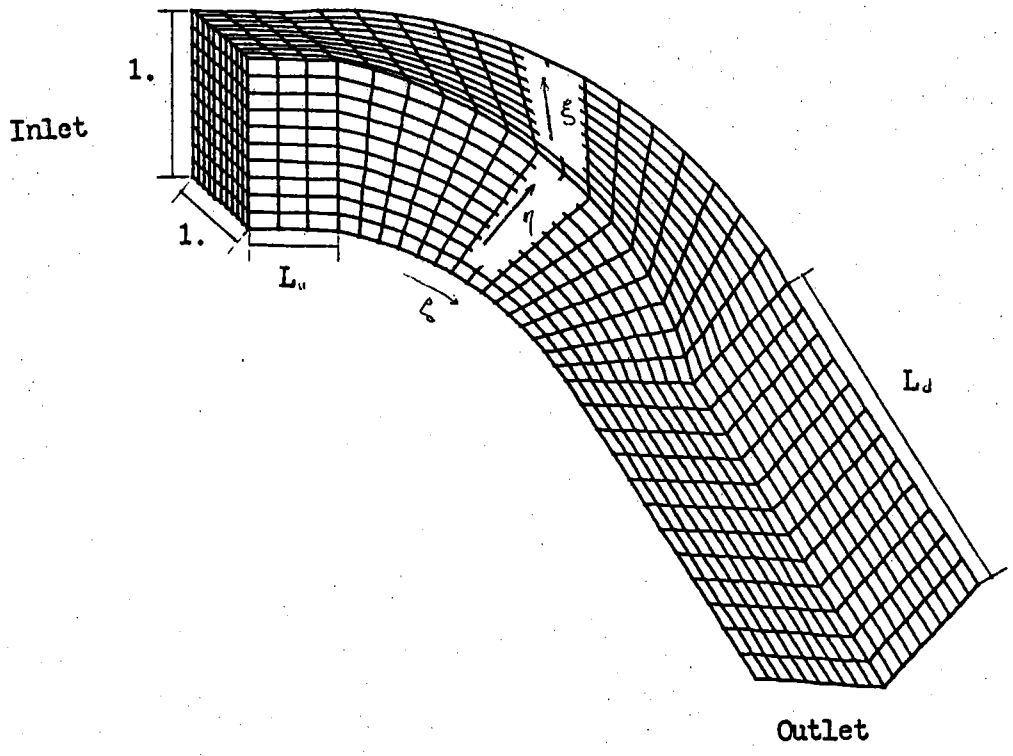

Fig.10 Description of the Twisted Square Elbow

L_u = 0.524, L_d = 2.10

Angle of Turning = 60

Angle of Twisting = 60

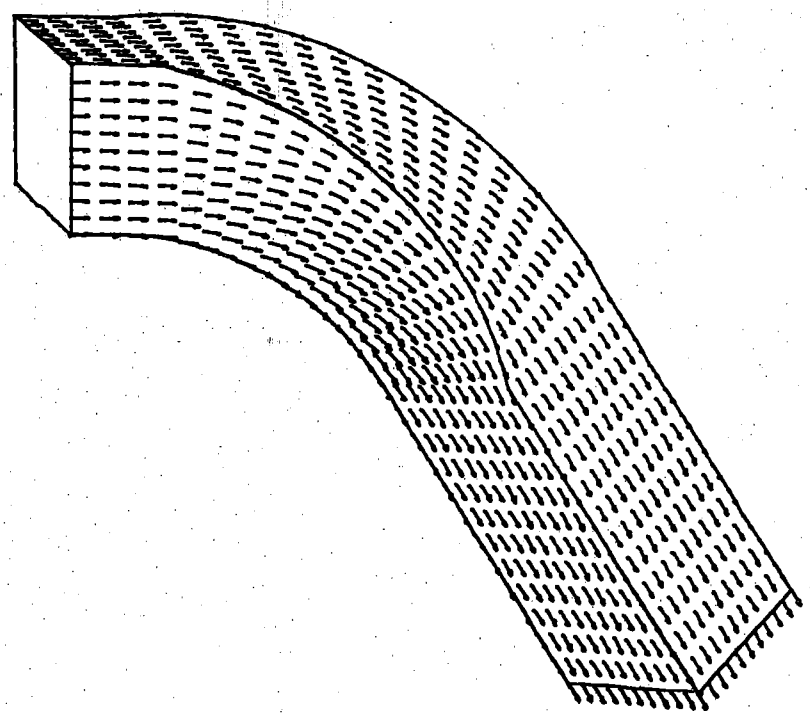

Fig.11 Potential Velocity distribution on Walls

Mesh = 11×11×31

Scale of V/V_* → = 1.0

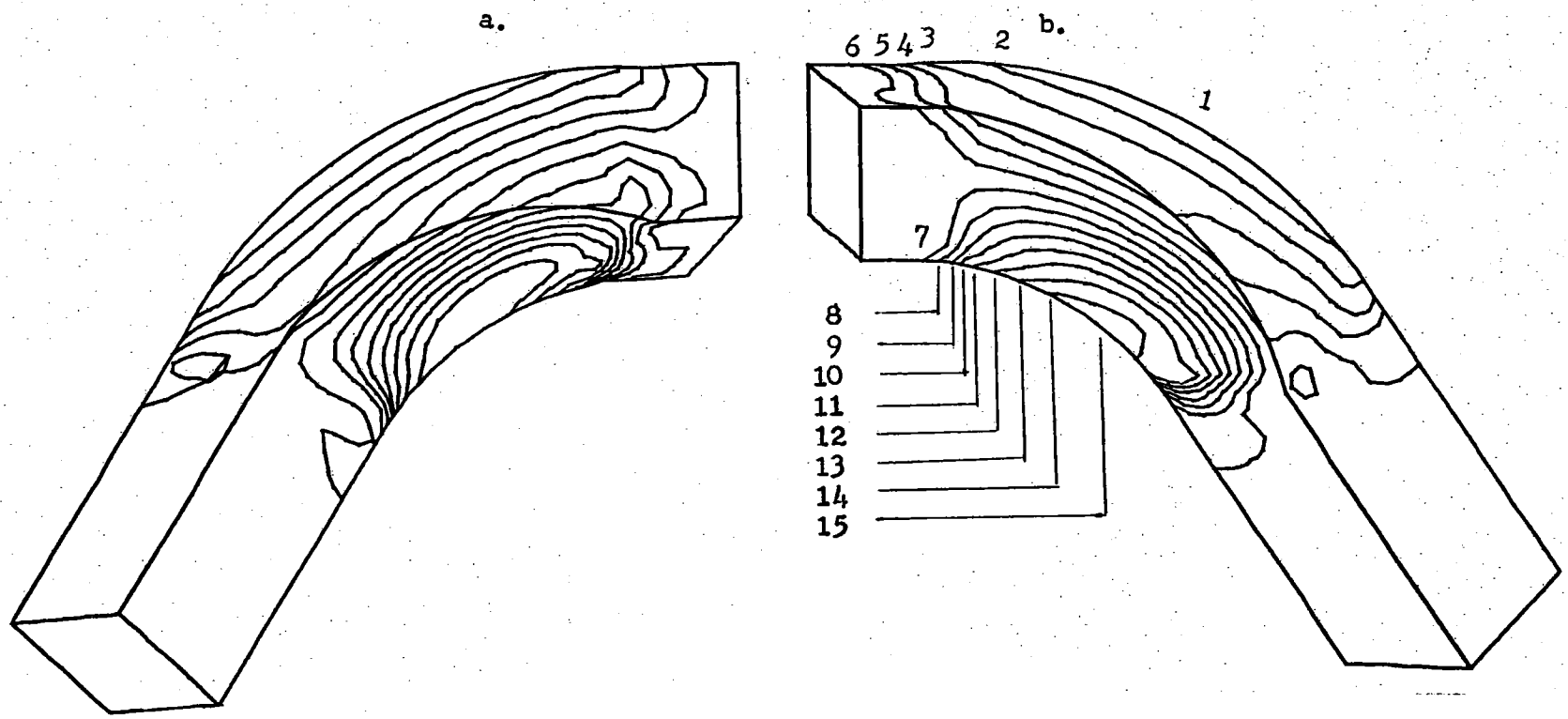

Fig.12 Potential Cp Distribution on Outermost Surfaces

a. View from Back

b. View from Front

Values of Contours:

1, 2, 3, ..., 15

-0.575, -0.503, -0.431, ..., 0.433

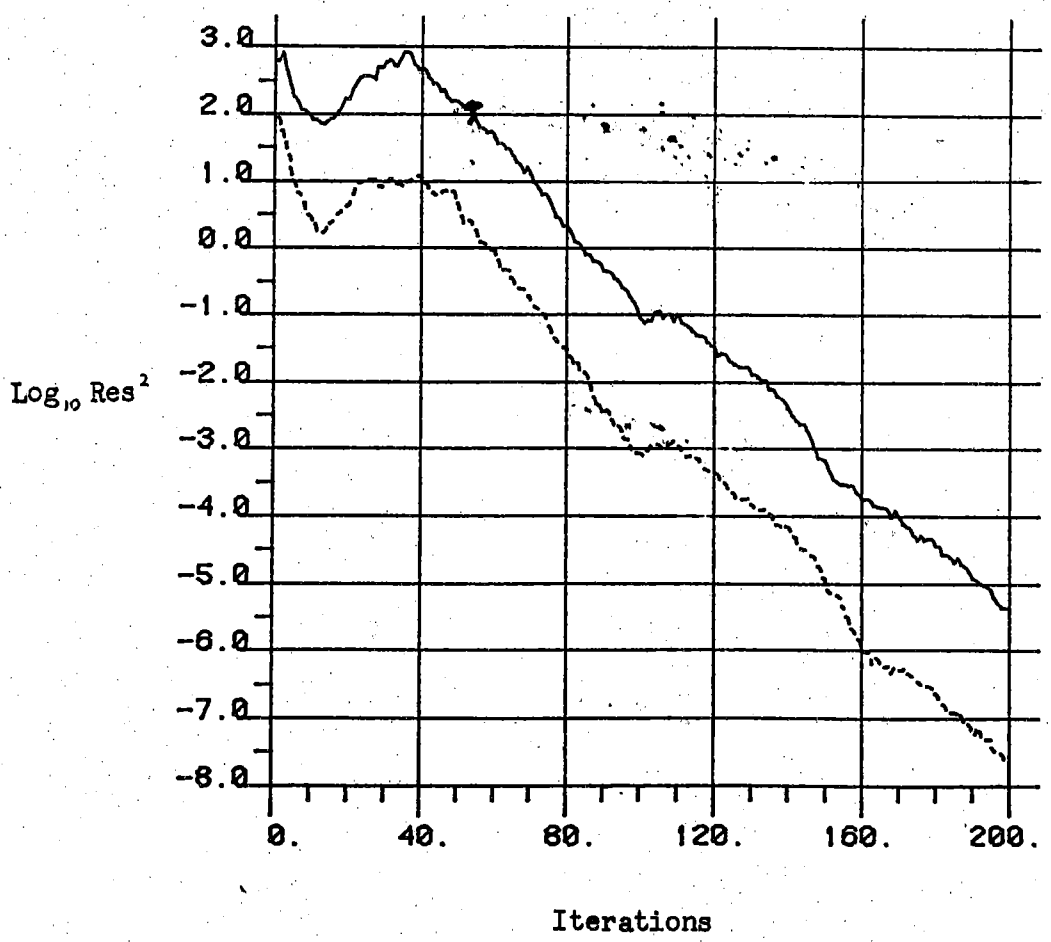

Fig.13 Residual Histories of W's and A's Eqs.

Mesh = 11x11x31, Re = 80

——— Residual from W's Eq.

------- Residual from A's Eq.

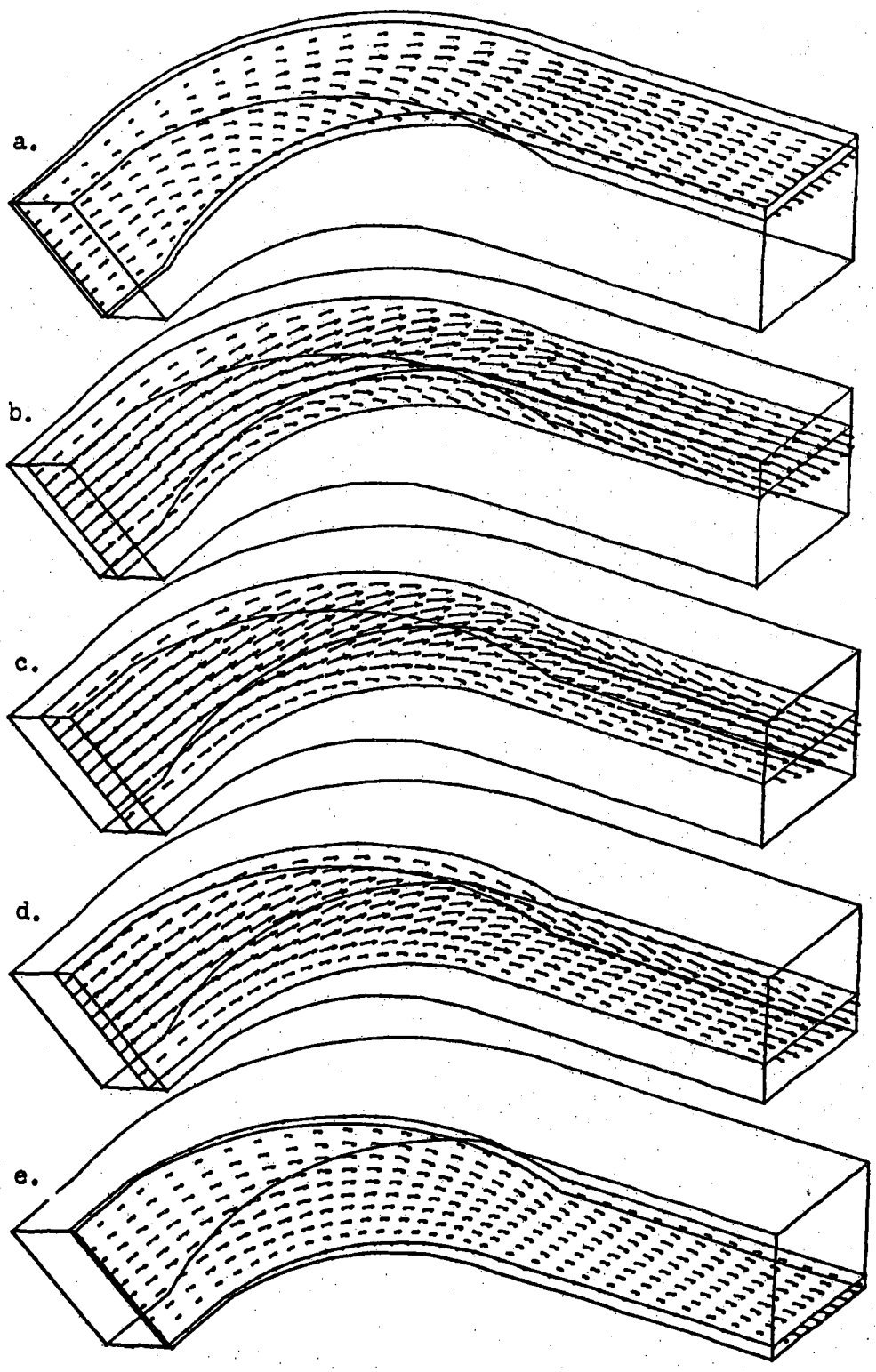

Fig.14 Velocity Distribution in =constant Surfaces

Mesh = 11x11x31, Re = 80

Scale of V/v_* → = 1.0

a.

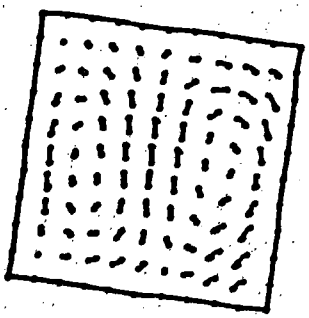

b.

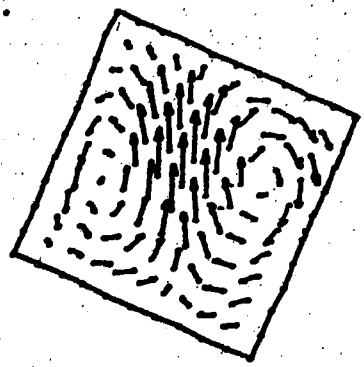

c.

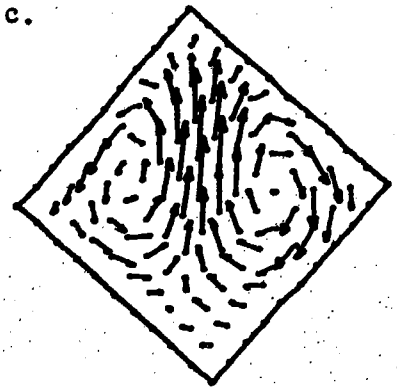

d.

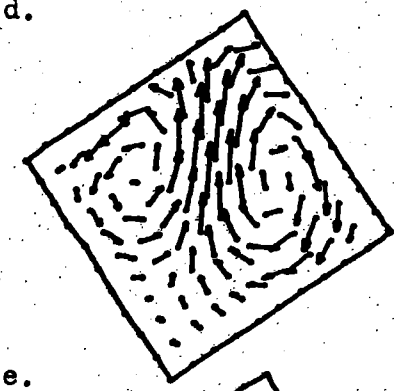

e.

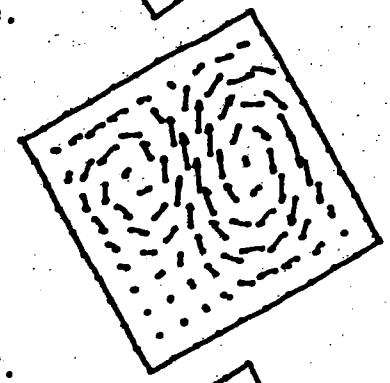

f.

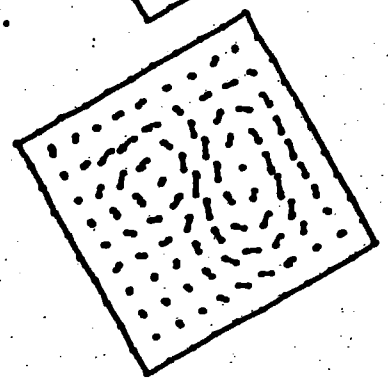

g.

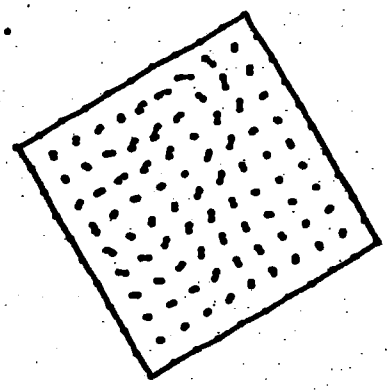

Fig.15 Development of Secondary Flow

Mesh = 11×11×31, Re = 80

Scale of V/v → = 0.2

a. In the Section of $\theta = 8^\circ$

b. In the Section of $\theta = 24^\circ$

c. In the Section of $\theta = 40^\circ$

d. In the Section of $\theta = 56^\circ$

e. In the Section of 1/4 Downstream Tangent

f. In the Section of 7/12 Downstream Tangent

g. In the Outlet